

# Kinematic Couplings for Synchrotron Radiation Instrumentation

S. Zelenika and S. Flechsig\*

*Paul Scherrer Institut – Swiss Light Source, CH - 5232 Villigen PSI, Switzerland  
Phone: + 41 - (0)56 – 3104586; Fax: + 41 - (0)56 – 3102549  
E-mail: sasa.zelenika@psi.ch*

*\*EU Project “Handling and Assembly of Functionally Adapted Microcomponents,”  
c/o Sincrotrone Trieste S.C.p.A., Strada Statale 14 - km 163.5 in AREA Science Park,  
I - 34012 Basovizza (TS), Italy*

## Abstract

Kinematic couplings are often used in synchrotron radiation facilities to achieve high-precision positioning and relocation of opto-mechanical components. The analytical and numerical modeling of their stress-strain behavior is however difficult, as it implies the necessity to deal with the Hertz theory of point contacts between elastically deforming solids.

This work addresses the limits of applicability of the analytical approaches available in literature for the calculation of high-precision kinematic couplings. The validity of the theoretical models, as well as the achievable repeatability of the couplings, is assessed experimentally for various loading conditions and material types.

**Keywords:** kinematic mounts, Hertzian contact, high-precision, x-ray equipment

## 1. Introduction

Kinematic couplings (Fig. 1) are well suited for high-precision applications such as the precision positioning and relocation of opto-mechanical components, metrological applications, scientific apparatuses, the assembly of microparts as well as the high-precision manufacturing systems and machine tools [1,2]. At synchrotron radiation (SR) facilities, kinematic mounts are often used to obtain independent and reproducible position adjustment of beamline components, especially those to be removed for servicing and precisely relocated to their original positions (e.g. end-stations and front-end components). The adoption of kinematic mount principles has in fact resulted in significant reductions of the time spent in aligning the SR devices and an increase of the time spent using them (acquiring data) [3]. Kinematic couplings are in fact self-locating and free from backlash, allowing re-positioning repeatabilities in the micrometric and sub-micrometric range to be attained in static, but also in applications involving dynamic forces [1-3]. These devices can accommodate differential thermal growths, keeping the resulting mechanical stresses to a minimum. They are not very sensitive to contamination and do not require an extensive wear-in period. Kinematic mounts are also characterized by limited costs, since their repeatability is orders of magnitude bigger than the accuracy to which they are manufactured. Moreover, since they are not overconstrained, their behavior can be represented in a closed form solution [1,2].

The main drawback of kinematic couplings is that, with only six contact points, they present high contact stresses (cf. [3]), which are difficult to calculate both analytically and numerically. In fact, the analysis of such devices implies the necessity to consider the non-linear Hertz theory of point contacts between elastically deforming

solids [4]. In literature various approaches can be traced which deal with such a problem. The exact model based on the theory of elasticity is complex since it involves an iterative evaluation of elliptic integrals [5]. The other approaches are based on approximated methods that make use of diagrams [6, 7], polynomial approximations [8] or interpolating procedures [6,9,10] for the calculation of the stress-strain behavior of the bodies in contact as function of the mechanical characteristics and main dimensions of the coupling.

The aim of this work is to establish the limits of applicability of the analytical approaches available in literature depending on the required degrees of accuracy. The validity of the theoretical models is then assessed experimentally via high-precision measurements. These allow the influence of the various mechanical parameters on the behavior of kinematic couplings to be established.



Fig. 1: 3-V groove kinematic mount.

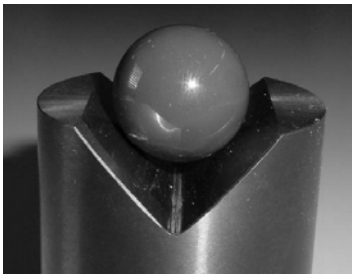


Fig. 2: A ball in a V groove.

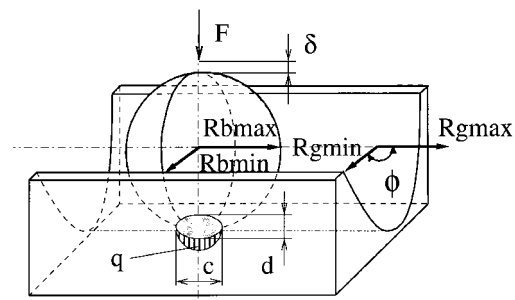


Fig. 3: Model parameters.

## 2. Analytical Models

Two kinematic mount configurations are applied in praxis: the cone-V-flat (Kelvin clamp) configuration, and the 3-V groove (Maxwell mount) configuration. In this work 3-V groove kinematic couplings (Fig. 1) are considered, since they are characterized by several advantages that make them suited for high-precision applications i.e., [1,8]:

- a symmetric arrangement is maintained,
- simpler manufacturing (reduced manufacturing costs) is assured,
- higher dynamic stability is obtained (the stress state in the mount is minimized),
- uniform contact stresses are assured, and
- thermal expansion takes place around a central point.

In this case the treated problem therefore reduces to the study of the stress-strain behavior of a ball in a groove (Fig. 2).

The analytical model describing the non-linear behavior of point contacts between elastically deforming isotropic solids loaded perpendicular to the surface (shear stress,

i.e. friction, is neglected), in which the dimension of the contact area is small compared to the radii of curvature and the dimensions of the involved bodies, known as the Hertzian model [4-6,8,11], is often employed in engineering practice (e.g. for ball bearing, gear couplings and locomotive wheels studies). The corresponding exact analytical model entails, however, a lengthy iterative evaluation of transcendental equations involving the complete elliptic integrals of the first and second kind (Fig. 4). In fact, by indicating with  $E_1$  and  $E_2$  the Young's moduli of the bodies in contact, with  $F$  the normal contact load (Fig. 3), with  $\nu_1$  and  $\nu_2$  the Poisson's ratios of the bodies, with  $R_b$  the ball radius ( $R_b=R_{b\ min}=R_{b\ max}$ ) and with  $R_{g\ min}$  the groove radius ( $R_{g\ max}=\infty$ ), the following notation can be introduced [5]:

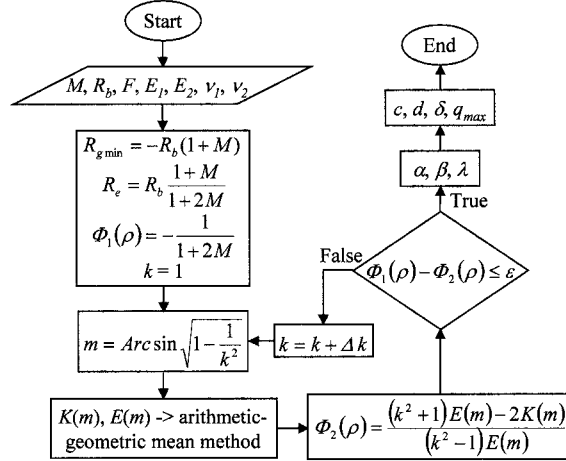


Fig. 4: Exact analytical model.

- equivalent Young modulus:

$$E_e = \frac{1}{\frac{1-\nu_1^2}{E_1} + \frac{1-\nu_2^2}{E_2}}, \quad (1)$$

- ratio of groove and ball radii of curvature and equivalent radius:

$$M = -\left(\frac{R_{g\ min}}{R_b} + 1\right) \quad R_e = R_b \frac{1+M}{1+2M}, \quad (2)$$

- curvature difference:

$$\Phi(\rho) = -\frac{1}{1+2M} = \frac{(k^2+1)E(m) - 2K(m)}{(k^2-1)E(m)} \quad (\text{with } \rho = \frac{1}{R_e}), \quad (3)$$

- ratio of the major and minor semiaxes lengths of the elliptical contact area (Fig. 3):

$$k = \frac{c}{d} \geq 1. \quad (4)$$

The resulting calculation algorithm is then arranged as shown on Fig. 4, where

$$\alpha = \sqrt[3]{\frac{2k^2 E(m)}{\pi}} \quad \beta = \sqrt[3]{\frac{2E(m)}{\pi k}} \quad \lambda = \frac{2K(m)}{\pi} \sqrt[3]{\frac{\pi}{2k^2 E(m)}}, \quad (5)$$

are the characteristic parameters, while

$$K(m) = \int_0^{\pi/2} \frac{d\varphi}{\sqrt{1-m\sin^2\varphi}} \quad E(m) = \int_0^{\pi/2} \sqrt{1-m\sin^2\varphi} \, d\varphi, \quad (6)$$

are the complete elliptic integrals of the first and second kind.

The results of the algorithm represent then the major ( $c$ ) and minor ( $d$ ) semiaxes of the elliptical contact area, the interpenetration distance  $\delta$  of the bodies in contact (distance of approach of two far-filed points in the bodies) and the maximum contact stress  $q_{max}$ :

$$c = \alpha \sqrt[3]{\frac{3F R_e}{2E_e}} \quad d = \beta \sqrt[3]{\frac{3F R_e}{2E_e}} \quad \delta = \frac{\lambda}{2R_e} \sqrt[3]{\frac{3F R_e}{2E_e^2}} \quad q_{max} = \frac{3F}{2\pi c d} \quad (7)$$

The approximated methods given in literature in which the need to calculate the elliptic integrals is obviated by introducing polynomial [8], tabular [6,9,10] or graphical [6,7] representations of the characteristic parameters are summarized in Table 1, where  $a$  is the radius of the circular contact area,  $\alpha$ ,  $\beta$ ,  $\gamma$ , and  $\lambda$  are the characteristic parameters (of different value for the various considered methods),  $\cos\theta$  is dependent on the radii of curvature and  $\phi$  - the angle between the planes of principal curvature (Fig. 3), while the other parameters are analogous to those of the exact analytical model given above.

Table 1: Approximated Analytical Methods

	pol. approx. [8]	interp. [9]	interp. [10]	diagrams [7]	diagrams [6]	gap-bending hyp. [8]
$R_c$	$R_c = R_b \frac{1+M}{1+2M}$	$R_c = 2R_b \frac{1+M}{1+2M}$	$R_c = 1.5R_b \frac{1+M}{1+2M}$	$R_c = R_b \frac{1+M}{1+2M}$	$R_c = 4R_b \frac{1+M}{1+2M}$	$R_c = R_b \frac{1+M}{1+2M}$
$\cos\theta$	$\cos\theta = \frac{R_e}{ R_{g\min} }$	$\cos\theta = \frac{R_e}{2 R_{g\min} }$	$\cos\theta = \frac{R_e}{1.5 R_{g\min} }$	$\cos\theta = \frac{R_e}{ R_{g\min} }$	$\cos\theta = \frac{R_e}{4 R_{g\min} }$	/
$c$	$c = \alpha \sqrt[3]{\frac{3F R_e}{2E_e}}$	$c = \alpha \sqrt[3]{\frac{3F R_e}{4E_e}}$	$c = \alpha \sqrt[3]{\frac{F R_e}{E_e}}$	$c = \alpha \sqrt[3]{\frac{F R_e}{E_e}}$	$c = \alpha \sqrt[3]{\frac{3F R_e}{8E_e}}$	$c = a = \sqrt[3]{\frac{3F R_e}{2E_e}}$
$d$	$d = \beta \sqrt[3]{\frac{3F R_e}{2E_e}}$	$d = \beta \sqrt[3]{\frac{3F R_e}{4E_e}}$	$d = \beta \sqrt[3]{\frac{F R_e}{E_e}}$	$d = \beta \sqrt[3]{\frac{F R_e}{E_e}}$	$d = \beta \sqrt[3]{\frac{3F R_e}{8E_e}}$	$d = a = \sqrt[3]{\frac{3F R_e}{2E_e}}$
$\delta$	$\delta = \lambda \sqrt[3]{\frac{2F^2}{3R_e E_e^2}}$	/	$\delta = \lambda \sqrt[3]{\frac{F^2}{R_e E_e^2}}$	$\delta = \lambda \sqrt[3]{\frac{F^2}{R_e E_e^2}}$	$\delta = \lambda \sqrt[3]{\frac{9F^2}{64R_e E_e^2}}$	$\delta = \frac{1}{2} \sqrt[3]{\frac{9F^2}{4R_e E_e^2}}$
$q_{max}$	$q_{max} = \frac{3F}{2\pi c d}$	$q_{max} = \frac{3F}{2\pi c d}$	$q_{max} = \frac{3F}{2\pi c d}$	$q_{max} = \gamma \sqrt[3]{\frac{F E_e^2}{R_e^2}}$	$q_{max} = \frac{3F}{2\pi c d}$	$q_{max} = \frac{a E_e}{\pi R_e}$

The results obtained with the exact approach are compared in Fig. 5 with the approximated analytical methods. For clarity reasons, the results are given as differences of each of the considered method with respect to the exact solution. It can thus be observed that the gap-bending hypothesis [8], in which the contact between two curved surfaces is reduced to that of a plane and an equivalent sphere, introduces considerable errors. It is worth noticing, however, that this hypothesis yields conservative results.

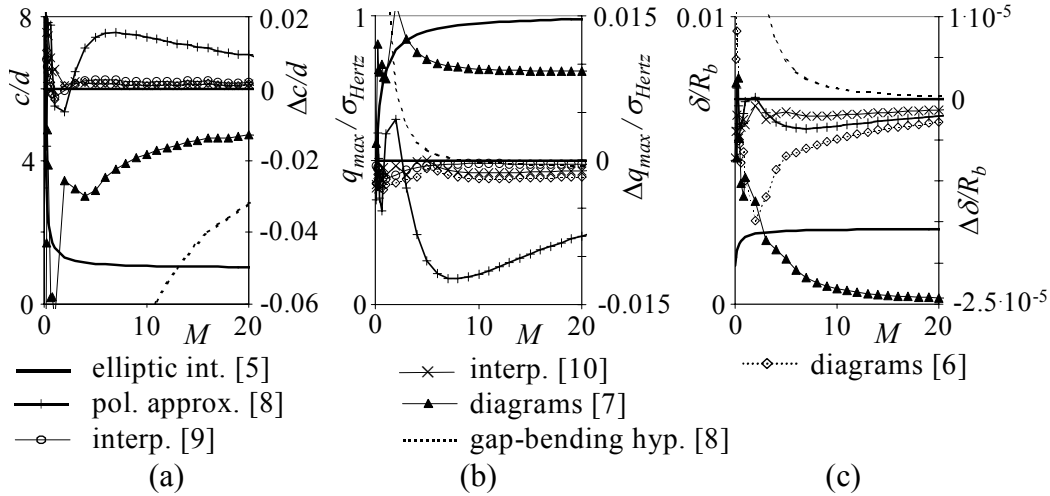


Fig. 5: Ratio of the semiaxes widths of the elliptical contact area (a), contact stresses normalized with respect to the Hertz stress  $\sigma_{Hertz}$  (b) and normalized interpenetration distances (c) versus the ratio of the radii of curvature  $M$ .

The errors introduced by the approximated methods based on polynomial, tabular and graphical representations are always smaller than  $\pm 2\%$  (or even, for the methods given in [9, 10],  $\leq \pm 0.2\%$  - Fig. 5). Given, however, the small entity of the stresses and strains involved in most high-precision applications of kinematic mounts, in absolute terms these errors are negligible in all but those cases in which true nanometric accuracies are sought. Only in the case when the mentioned characteristic parameters approach their limit values (respectively 0 and  $\infty$ ), which physically corresponds to the case when the curvature of the groove approaches that of the ball, the errors involved in the approximated methods become appreciable. In this case, however, the basic assumptions of the Hertzian model do not hold any more, and the Hertz theory itself starts to break down [8].

### 3. Experimental Assessment

#### 3.1 Experimental Set-Up

In high-precision applications the repeatability of the couplings has to be addressed [8]. On the other hand, the considered analytical approaches cannot take into account the extent of non-repeatability caused by friction (friction affects not only repeatability, but also the kinematicity, the stiffness and the centering ability of the couplings), as this effect can be evaluated only with elaborated numerical formulations based on incremental variational inequalities [12]. Even in that case, however, the extent of variation due to the stochastic nature of friction is not taken into account. Moreover, since the magnitude of the deflections is often in the submicron range, surface finish plays an important role. In fact, real solids make contact only where the asperities on the two surfaces come together, and therefore Hertzian analysis is merely the limit case to which real contacts tend [13]. Other effects, such as load asymmetry, also affect the repeatability of the couplings.

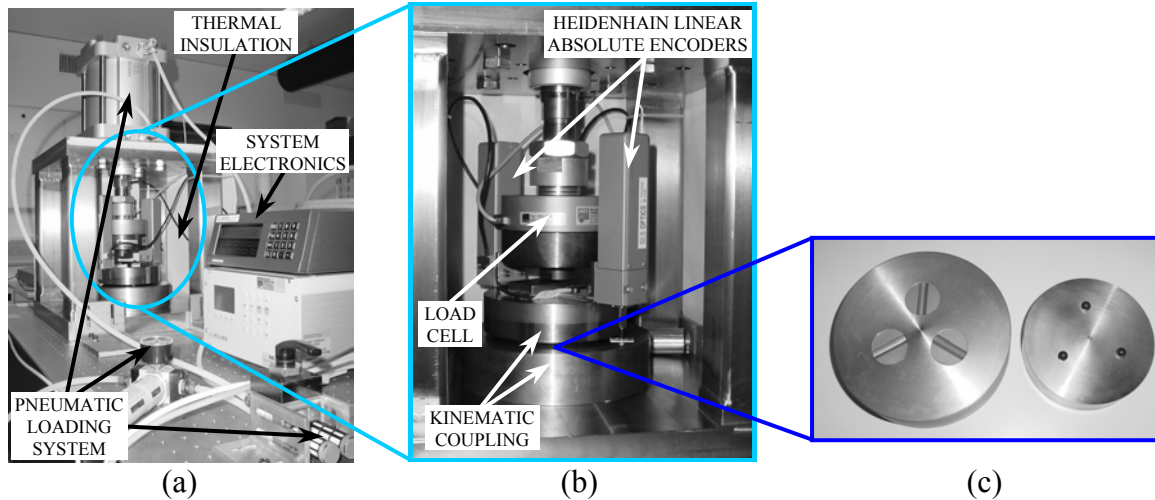


Fig. 6: Experimental set-up (a) with detail of the load and displacement measurement systems (b) and of the kinematic coupling elements (c).

In order to examine thus the repeatability and, as the most important feature for high-precision applications, the interpenetration distance of the couplings, an experimental set-up was built (Fig. 6). Gothic-arch shaped grooves ( $R_{g \min}=12 \text{ mm} \div \infty$ ) with polished contact surfaces ( $R_a=100 \text{ nm}$ ) are built as modular inserts and epoxied onto the lower coupling plate. For balanced stiffness in all directions, the angle of inclination of the grooves was chosen to be  $45^\circ$ , while good stability and overall stiffness is obtained by choosing the coupling configuration where the normals to the planes of the contact force vectors bisect the angles of the triangle formed by the balls that lie in the grooves. In order to make the compliance of balls' fixation low compared to that of the coupling, the balls ( $R_b=5.5 \div 10 \text{ mm}$ ,  $R_a=20 \div 60 \text{ nm}$ ) are inserted into conical seats at the upper coupling plate, burnished until the surface is brinelled, and then epoxied [8].

The set-up is thermally isolated (a stability of  $\pm 0.1^\circ\text{C}$  was reached). Stainless steel grooves and balls of various hardness (HRC34 $\div$ 67) are used. To minimize fretting corrosion, friction, as well as the footprint (i.e. to approach as much as possible true point contacts) [8], ceramic (WC and  $\text{Si}_3\text{N}_4$ ) grooves and balls are also employed. The loads are applied to the coupling via a pneumatic piston, and their magnitudes are measured with a precision ( $\pm 0.25\%$  ES) calibrated load cell. The interpenetration distance is measured with linear absolute encoders (HEIDENHAIN type CT 6002, resolution: 5 nm, accuracy:  $\pm 100 \text{ nm}$ ). Two encoders are used to have control of the symmetry of behavior.

### 3.2 Results and Discussion

The results of typical cyclic measurements and the corresponding theoretical data calculated by using the exact analytical model are shown in Fig. 7. The reported values are 25 cycle averages (with 100 points taken in each cycle). The shown interval of uncertainty (up to  $\pm 10\%$  of the measured values) is mainly due to the dimensional tolerances of the couplings' components, the residual compliances (e.g., the epoxied connections) and the uncertainty in the mechanical properties of the used materials (cf. [9]). Despite the care devoted to the set-up of the experimental apparatus, this uncertainty

is hence much larger than the errors introduced by the adoption of the approximated analytical methods outlined above.

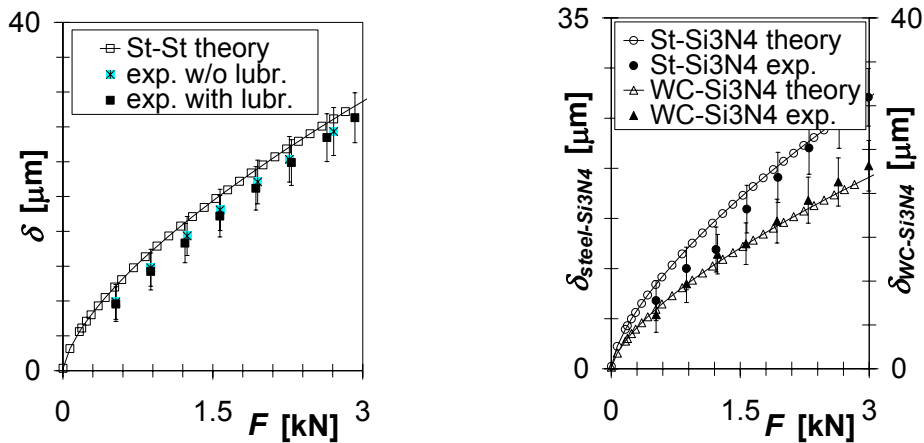


Fig. 7: Comparison of theoretical and experimental results for different materials.

The obtained results can be summarized as:

- In all the considered cases, the theoretical values are within the intervals of uncertainty of the measurements, regardless of the used materials. For small loads the measured values are smaller than the theoretical ones, which could be due to the surface roughness and the resulting flattening of the contact points (“micro-approaching” [5]). This is supported also by the observed brinelling of the surfaces in contact (Fig. 8). In fact, previous studies have allowed to establish that because of the surface roughness, for light loads the peak pressure can be only 1/3 of the theoretical one, while the contact area can in turn be up to 10 times larger than in theory [13]. It should also be noticed that the micro- and nano-hardness and Young’s moduli differ from the macroscopic ones and depend on the state of the surface [14], which can have a significant impact on the results in this region, too.
- For higher loads the experimental results are generally closer to the theoretical ones, which could be due to the relatively lower influence of the surface finish and the residual compliances. In this case, by using ceramic coupling components, a tendency towards higher measured interpenetration distances than those calculated theoretically was observed. This behavior could be due to the uncertainty in the mechanical properties of ceramic materials.
- Although lubrication generally has a small effect (cf. Fig. 7), in some instances it can induce a lowering of the measured values of up to 10%. The explanation for this occurrence was not found.

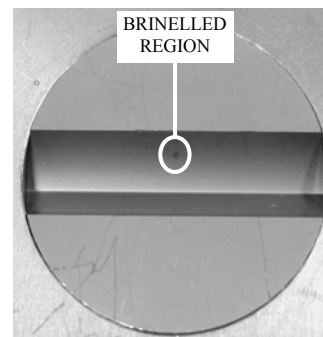


Fig. 8: Brinelling of the contact surface.

- Usage of softer materials (HRC34 steel) causes plastic deformations even for small loads. This increases the contact area, hence lowering the resulting interpenetration distances far below the theoretical values.
- After a wear-in period of  $\leq 50$  cycles, the repeatability of the couplings is typically in the  $\sigma \leq 100$  nm range i.e., comparable to the surface finish of the coupling interface. The residual non-repeatability could be due not only to surface finish, but also to non-linearities such as creeping [11] or pre-sliding displacement effects [15].

A trial was performed also to measure the area of the contact region by optical means. The measurement was performed by employing a 3D ZYGO type Newview 5010 scanning-white-light-interferometry-based surface profiler used to characterize the polishing accuracy of optical surfaces (vertical resolution: 0.1 nm, RMS repeatability: 0.4 nm, lateral resolution: 4.72  $\mu\text{m}$ ). It was hence shown that:

- ▶ In the elastic domain the results are characterized by low accuracy and big dispersion.
- ▶ In the plastic domain, the best results are obtained by applying a thin (ca. 50 nm) graphite coating to the contact area. Although a good accuracy is obtained, the results are of little practical use.
- ▶ Previous trials to measure the contact area by using contact resistance measurements [16] or techniques based on photoelasticity [11] have also given results characterized by low accuracy. The usage of newly developed pressure sensitive films [17] could allow to improve the situation in this regard.

#### 4. Conclusions

Except for the gap-bending hypothesis method, the approximated analytical approaches available in literature for the evaluation of the stress-strain behavior of kinematic couplings are giving results equivalent to those obtained with the exact analytical model in the micrometric and sub-micrometric domain, and are therefore of suitable accuracy for most of the practical cases encountered in dimensioning high-precision kinematic couplings.

In the whole range of elastic deformations, the correspondence of the theoretical values of the interpenetration distances with the experimental ones is within the intervals of uncertainty of the latter, regardless of the used materials and lubrication conditions. These effects seem, in fact, to influence the behavior only in the submicrometric range.

The repeatability of the couplings is comparable to the surface finish of the contact interface and thus it is in the 100 nm range.

The measurements of the contact area are characterized by a low accuracy and are left to a future study where newly developed pressure sensitive films will be employed.

## 5. References

- [1] A. H. Slocum, “Kinematic couplings for precision fixturing, Part I,” *Prec. Eng.*, 10 (2), pp. 85-91 (1988).
- [2] A. H. Slocum and A. Donmez, “Kinematic couplings for precision fixturing, Part 2,” *Prec. Eng.*, 10 (3), pp. 115-122 (1988).
- [3] T. Oversluizen, W. Stoeber and E. D. Johnson, “Kinematic mounting systems for NSLS beamlines and experiments,” *Rev. Sci. Instr.*, 63 (1), pp. 1285-1288 (1992).
- [4] H. Hertz, “Gesammelte Werke - Band I,” J. Ambrosius Barth, Leipzig (1895).
- [5] T. A. Harris, “Rolling Bearing Analysis” – 3<sup>rd</sup> ed., John Wiley, New York (1991).
- [6] G. Jacazio and B. Piombo, “Meccanica applicata alle macchine,” L & B, Torino.
- [7] G. Jacazio, “Progettazione delle strutture meccaniche,” Eda, Torino (1985).
- [8] A. H. Slocum, “Precision Machine Design,” Prentice Hall, New Jersey (1992).
- [9] S. P. Timoshenko and J. N. Goodier, “Theory of Elasticity,” McGraw Hill (1970).
- [10] W. C. Young, “Roark’s Formulas for Stress and Strain,” McGraw-Hill (1989).
- [11] K. L. Johnson, “Contact Mechanics,” Cambridge U. Press, Cambridge (1985).
- [12] M. Li et al., “Linear Complementary Formulations Involving Frictional Contact for Elasto-Plastic Deformable Bodies,” *J. Appl. Mech.*, 64, pp. 80-89 (1997).
- [13] J. A. Greenwood and J. H. Tripp, “The Elastic Contact of Rough Spheres,” *J. Appl. Mech.*, pp. 153-159 (1967).
- [14] X. Liu, T. Bell, F. Gao and D. G. Chetwynd, “Characterisation of engineered surfaces by a multi-functional tribological probe microscope,” *Proc. 3<sup>rd</sup> Int. Conf. Eur. Soc. Prec. Eng. Nanotech.*, Eindhoven, NL, pp. 719-722 (2002).
- [15] S. Zelenika and F. De Bona, “Micro-Dynamic Behaviour of a Nanometer Positioning System,” in *Adv. Manuf. Sys. Techn.*, Springer Verlag, pp. 771-779 (1999).
- [16] J. Dyson and W. Hirst, “The True Contact Area Between Solids,” *Proc. Phys. Soc.*, B67, pp. 309-312 (1954).
- [17] URL: [www.sensorprod.com](http://www.sensorprod.com).